Catal Lett (2009) 133:307–313
DOI 10.1007/s10562-009-0174-x

Mesostructured CeO_2 as an Effective Catalyst for Styrene Synthesis by Oxidative Dehydrogenation of Ethylbenzene

Jie Xu · Lun-Cun Wang · Yong-Mei Liu · Yong Cao · He-Yong He · Kang-Nian Fan

Received: 7 September 2009 / Accepted: 24 September 2009 / Published online: 14 October 2009

Abstract A new type of mesostructured ceria material was synthesized via template-assisted precipitation method and tested for the oxidative dehydrogenation (ODH) of ethylbenzene to styrene by molecular oxygen. The effect of calcination temperature on the catalytic performances of the ceria catalysts has been investigated. Among the catalysts tested, the CeO_2-450 sample derived by calcination at 450 °C exhibited the highest ethylbenzene conversion (34%) and styrene selectivity (87%). Comparing the reaction rates for ODH of ethylbenzene (ca. 6.1 mmol ST g_{cat}^{-1} h^{-1} at 450 °C) with the highly active nanostructured carbon-based catalysts in the current literature confirmed the very high activity of these new materials. The superior catalytic performance of the CeO_2-450 sample can be attributed to its high specific surface area and enhanced redox properties as revealed by H_2-TPR measurements.

Keywords Ceria · Mesostructured · Oxidative dehydrogenation (ODH) · Ethylbenzene · Styrene

1 Introduction

Styrene (ST) is an important monomer extensively used in the chemical industry for the manufacture of polymers, copolymers, and reinforced plastics [1]. Commercially, ST is mainly produced by means of the direct dehydrogenation (DH) of ethylbenzene (EB) at high reaction temperature (600–650 °C), with potassium-iron oxide as a catalyst [2, 3]. Due to its highly endothermic nature, this conventional route suffers from several disadvantages such as intensive energy consumption and rapid coking. Alternatively, the oxidative dehydrogenation (ODH) of EB has attracted considerable recent attention since it can be operated at lower temperatures and the EB conversion would not be equilibrium limited [2, 4–6]. A range of catalysts have been reported for this process in the recent literature including amorphous $AlPO_4$ [1], $V_2O_5/CeO_2/Al_2O_3$ [2], CaO/SiO_2 [7], MnO_2/SiO_2 [8], $Mg(VO_4)_2$-MgO [9]. In particular, promising results have been obtained when using onion like carbon (OLC) [5, 10] or carbon nanofibers (CNF) [11, 12] as the ODH catalyst. Nevertheless, the industrial application of the carbon-based catalysts has been till now prevented by their fine powder nature and intrinsically low resistance to combustion of the material [13]. In this context, there is a great incentive to develop new robust catalyst applicable for the ODH of EB.

Ceria (CeO_2) is a key redox component in the catalyst formulations for many industrially important reactions, such as three-way-catalysts for automobile exhaust treatment [14, 15], CO_2 activation [16], CO oxidation [17] and low temperature water- gas shift reaction [18]. The success of ceria in various applications is largely attributed to its superior low temperature reducibility and remarkable oxygen storage/release capacities [2]. In the present work, we demonstrate for the first time that bulk CeO_2, previously established to be a useful promoter in catalytic systems such as Cr_2O_3/Al_2O_3 [19], V_2O_5/Al_2O_3 [2] and Fe_2O_3-Cr_2O_3-K_2CO_3 [8] for the direct EB dehydrogenation, could be active and selective for the ODH of EB. In particular, we

J. Xu · L.-C. Wang · Y.-M. Liu · Y. Cao (✉) · H.-Y. He · K.-N. Fan (✉)
Department of Chemistry, Shanghai Key Laboratory of Molecular Catalysis and Innovative Materials, Fudan University, 200433 Shanghai, People's Republic of China
e-mail: yongcao@fudan.edu.cn

K.-N. Fan
e-mail: knfan@fudan.edu.cn

have shown that the ODH of EB could proceed much more effectively over a template-derived mesoporous CeO_2 material with a surface area as high as 180 m^2 g^{-1}.

2 Experimental

2.1 Catalyst Preparation

Mesostructured ceria materials with high surface area were synthesized via a previous established template-assisted precipitation method [20]. Typically, a NaOH solution (1 g in 150 ml of distilled water) was added into a mixed solution of $Ce(NO_3)_3$ and CTAB (2.17 g of $Ce(NO_3)_3{\cdot}6H_2O$ and 1.09 g of CTAB in 100 ml of distilled water) under stirring. The mixture was then maintained in a sealed glass vessel under stirring for 5 days. After aging at 90 °C for 3 h, the as-obtained yellow precipitate was filtered and washed with hot water (~80 °C) for four times to remove the residual CTAB. The resultant yellow powder was dried at 100 °C for 6 h and then calcined at 450, 700, 800, and 900 °C for 4 h, respectively. The as-synthesized ceria samples are denoted as CeO_2-*T* where *T* stands for the calcination temperature.

2.2 Characterization

Nitrogen sorption at −196 °C was measured using a Micromeritics TriStar 3000 after the samples were degassed (1.33×10^{-2} Pa) at 300 °C overnight. The specific surface area was calculated using the BET method, and pore size distribution was determined by the BJH method.

Structural analysis of ceria samples was carried out on a Bruker D8 Advance X-ray diffractometer equipped with a graphite monochromator, operating at 40 kV and 40 mA and employing nickel-filtered Cu-Kα radiation ($\lambda = 1.5418$ Å).

Temperature programmed reduction (TPR) profiles were obtained on a homemade apparatus. 100 mg of the samples were pretreated in a mixed gas ($O_2/N_2 = 1/8$) at 300 °C for 30 min and cooled to room temperature. Subsequently, the samples were reduced with 5% H_2/Ar at 40 mL min^{-1} with a ramping rate of 5 °C min^{-1} to 910 °C. The H_2 consumption was monitored by a TCD detector.

Thermal gravimetric analysis (TGA), as well as temperature-programmed oxidation (TPO) measurements of the spent CeO_2-450 sample, were conducted on a Perkin-Elmer TGA 7 analyzer. The sample was placed in an α-Al_2O_3 cumber and heated in flowing air (50 mL min^{-1}) from room temperature to 800 °C at a rate of 20 °C min^{-1}.

2.3 Catalytic Activity Measurements

The activity of the catalysts for ODH of EB was measured in the temperature range of 350–550 °C at atmospheric pressure using a fix-bed, down-flow, tubular quartz reactor (i.d. 4 mm, length 400 mm). Each run used approximately 50 mg of catalyst in the form of 60-80-mesh particles, mixed with 300 mg of silicon carbide grains of similar size for best temperature control. EB was evaporated at 35 °C in flowing N_2 and subsequently mixed with O_2. Unless otherwise specified, the corresponding flow rate of EB, O_2, and N_2 is fixed at 0.5, 0.25 and 20 mL min^{-1}, respectively. Prior to testing, the catalysts were pretreated in a mixed gas ($O_2/N_2 = 1/8$) at 300 °C for 30 min. The products were analyzed by an on-line gas chromatograph (Agilent GC 6820 equipped with FFAP column for hydrocarbons and TDX-01 column for permanent gas analysis, coupled with FID and TCD detectors, respectively). The carbon balance closed to ± 5% and was additionally monitored by the CO_x content after catalytic combustion of organic species in a final total oxidation reactor [21].

3 Results and Discussion

3.1 Characterizations of Mesostructured Ceria Materials

The textural properties of the ceria annealed at 450, 700, 800 and 900 °C were studied by the N_2 sorption measurements. The values of specific surface area, mean pore diameter and pore volume are reported in Table 1. Figure 1a shows the pore diameter distribution and the

Table 1 Textural properties and TPR results of the ceria catalysts calcined at various temperatures

Catalysts	S_{BET} (m^2 g^{-1})	D_{pore} (nm)	V_{pore} (cm^3 g^{-1})	*d* (nm)[a]	H_2 consumption (mmol g^{-1})	
					Peak α[b]	Peak β
CeO_2-450	180	10.2	0.60	5.8	1.39 (96.5%)	0.05
CeO_2-700	128	9.6	0.52	7.9	0.80 (66.5%)	0.40
CeO_2-800	90	9.1	0.41	13.1	0.35 (36.1%)	0.62
CeO_2-900	55	8.9	0.22	18.5	0.23 (22.5%)	0.80

[a] Mean particle size of CeO_2 calculated by Sherrer equation base on the (110) diffraction peaks in the XRD patterns

[b] The data in the parenthesis are the percentage of peak α with respect to total H_2 consumption

corresponding adsorption–desorption isotherms of the CeO_2-450 material. According to the IUPAC classification, the isotherm can be classified as a type IV one, typical of mesostructured materials and the hysteresis loop is type H1 indicating a complex mesoporous structure. The pore size distribution (PSD) calculated from the desorption branch showed that the pore diameter ranges from 4 to 30 nm with a maximum at around 10.2 nm (the inset to Fig. 1a). Furthermore, it is seen that the specific surface area of the CeO_2-450 sample decreases continuously from 180 to 55 $m^2\ g^{-1}$ with increasing calcination temperature in the range of 450–900 °C. Note that the surfactant cannot be completely removed when the calcination temperature is lower than 450 °C. The loss of surface area after calcination at higher temperature may be caused by a partial collapse of the ceria pores [22, 23] along with the agglomeration of ceria particles as indicated by the XRD results presented below. Moreover, during our study, all the samples give no diffraction peak in the low-angle XRD patterns (not shown here), which are usually employed to verify the long-range ordering of mesopores. The absence of any ordered mesoporous structure in the as-synthesized CeO_2 is further supported by the TEM data as illustrated in Fig. 1b.

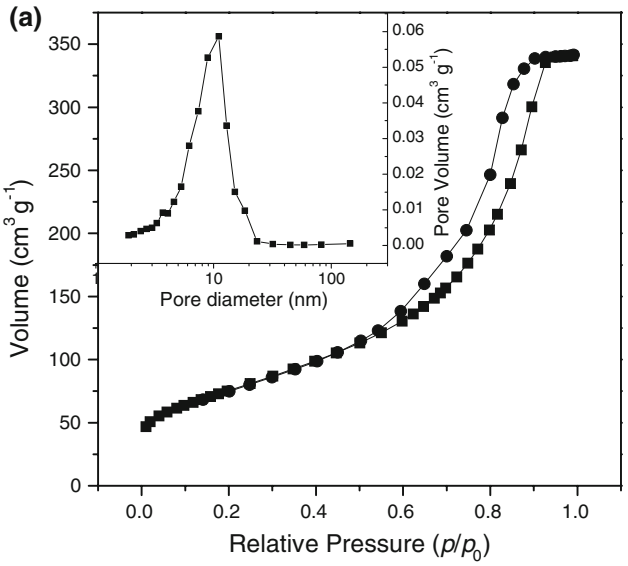

Fig. 1 N_2-sorption isotherm and pore size distribution **a** and corresponding TEM image **b** of CeO_2-450

Figure 2 shows the XRD patterns of the various ceria samples. The diffraction patterns of the mesostructured CeO_2-450 sample were found to be very broad, showing a semicrystalline nature of this material. The samples derived by calcination at higher temperatures presented a well crystallized phase. The peak intensities and their 2θ angles have been identified as characteristic of the cubic fluorite structure of CeO_2 (JCPDS no. 34-0394). As the calcination temperature increases from 450 to 900 °C, the diffraction peaks become stronger and sharper, indicating that the crystallinity is continuously improved. The average crystallite size of the CeO_2 sample was estimated from the half-height width of the (111) signal by using the Scherrer equation and given in Table 1. The crystallite size of ceria was within nanoscale which increased from 5.8 to 18.5 nm as the calcination temperature was raised from 450 to 900 °C.

TPR experiments were then carried out to investigate the reducibility of various ceria samples as shown in Fig. 3. The CeO_2-450 sample exhibits a broad low-temperature (LT) reduction profile from 250 to 600 °C (hydrogen consumption ca. 1.39 $mmol_{H2}\ g^{-1}$), a feature signifying superior low temperature reducibility [23]. In contrast, two main reduction peaks have been identified for the samples

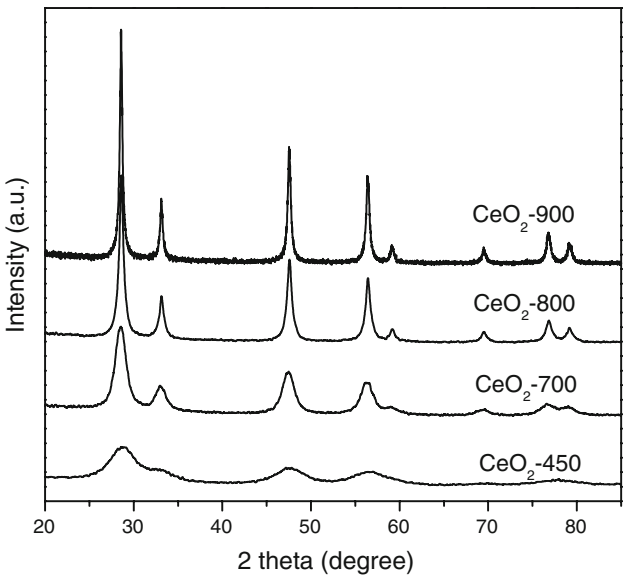

Fig. 2 XRD patterns of various ceria catalysts

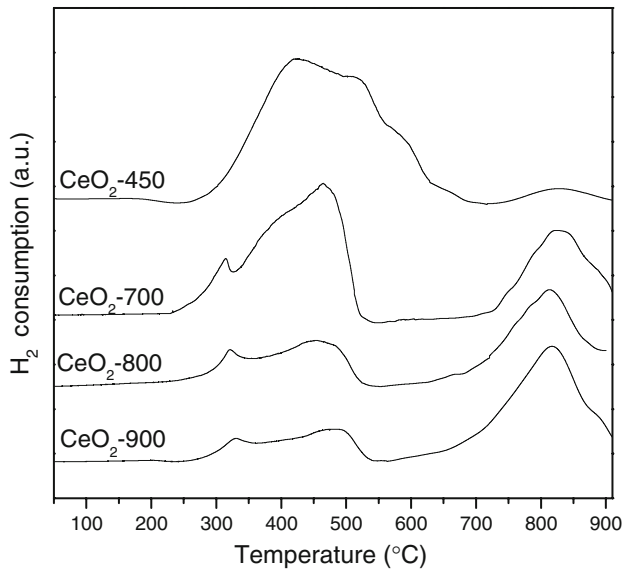

Fig. 3 H_2-TPR profiles of various ceria catalysts

calcined at higher temperatures: peak α (ca. 460 °C) and peak β (ca. 840 °C), which are generally attributed to the reduction of surface-capping oxygen and bulk oxygen species, respectively, [24–26]. Recently, based on the presumption that the TPR profile in ceria is not controlled by rate of oxygen diffusion from bulk to surface, Trovarelli et al. [27] proposed an alternative model to assign the two reduction peaks of CeO_2. Namely, the peak at lower and higher temperature was caused by the reduction of small and large ceria crystallites, respectively. Therefore, the highest fraction (96.5%, Table 1) of peak α for CeO_2-450 suggests that it has the smallest crystallite size, in line with the XRD data as reported in Table 1. Similarly, due to its largest crystallite size and lowest surface area resulting from higher calcination temperature, CeO_2-900 presents the highest percentage of peak β (77.5%, Table 1). Furthermore, the evolution trend of BET surface area is in parallel with that of the H_2 consumption of peak α, i.e., the larger surface area of ceria material, the larger amount of the low-temperature H_2 consumption [28].

3.2 Catalytic Performance in the ODH of EB

The activities of the present mesostructured ceria-based catalysts were explored under steady-state conditions between 350 and 550 °C, with a constant space velocity (415 mL g^{-1} min^{-1}) and EB/oxygen/nitrogen (1/0.5/40) ratio. The catalytic performances in terms of EB conversion, selectivity and ST yield for various ceria catalysts measured at reaction temperature of 450 °C were summarized in Table 2. The major component of the products over all ceria catalysts are ST (more than 80%), accompanied by appreciable amounts of CO_x and very small amount of other byproducts such as benzaldehyde and methyl benzyl alcohol. The results in Table 2 point to a remarkable effect of calcination temperature on the catalytic activity and selectivity to ST of the ceria material, viz. higher calcination temperature leads to lower activity and selectivity of the catalysts. The highest catalytic performance was obtained on CeO_2-450 with EB conversion of 34.1%, ST selectivity of 87.4% and ST yield of 29.8%.

Figure 4 illustrates the effect of reaction temperature on the activity and selectivity of the CeO_2-450 catalyst. The EB conversion increased rapidly with the reaction temperature up to 450 °C and then leveled off, with the selectivity of ST decreases smoothly from ca. 93–85%. Presumably, higher temperature should give rise to better catalytic activity for the ODH reaction. However, as described above, higher reaction temperature may also lead to the sintering or growth of CeO_2 particles, which can greatly compromise the activity of CeO_2-450 under these conditions. Moreover, a control experiment investigating the direct dehydrogenation of EB at the same reaction conditions in the absence of O_2 demonstrated that EB was poorly converted although the selectivity to ST was fairly high. The effect of O_2 concentration on the ODH of EB over CeO_2-450 can be further seen from Fig. 5. One can see that the stoichiometric concentration of oxygen (O_2/EB = 1/2) is the ratio of choice.

The evolution of the catalytic performance at 450 °C as a function of reaction time for the four ceria catalysts is shown in Fig. 6. The ST selectivity for all catalysts

Table 2 Catalytic performances of ceria catalysts calcined at various temperatures

Catalysts	Conversion of EB (%)[a]	Selectivity (%)			Yield of ST (%)	STY ($mmol_{ST}$ $g^{-1}_{catal.}$ h^{-1})
		ST	CO_x	Others[b]		
CeO_2-450	34.1	87.4	10.4	2.2	29.8	8.0
CeO_2-700	22.5	83.5	16.2	0.3	18.8	5.0
CeO_2-800	19.4	82.0	18.0	–	15.9	4.2
CeO_2-900	15.1	80.2	19.8	–	12.1	3.2

[a] Reaction condition: 450 °C, 50 mg catalyst, initial activity data collected at the reaction time of 0.5 h

[b] Benzene, benzaldehyde or methyl benzyl alcohol

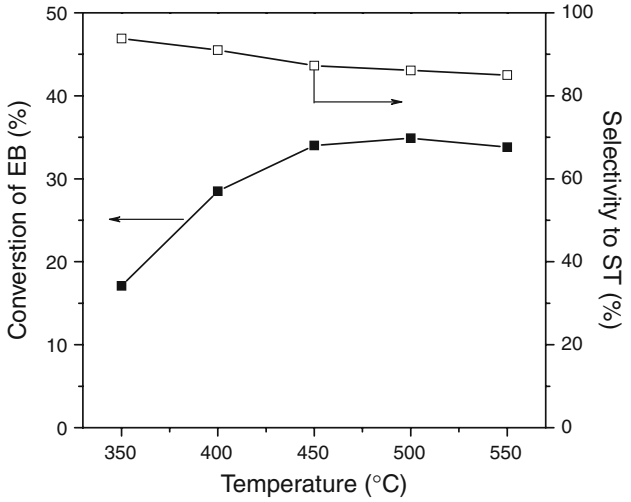

Fig. 4 Effect of reaction temperature on the activity and selectivity of CeO_2-450 in ODH of EB

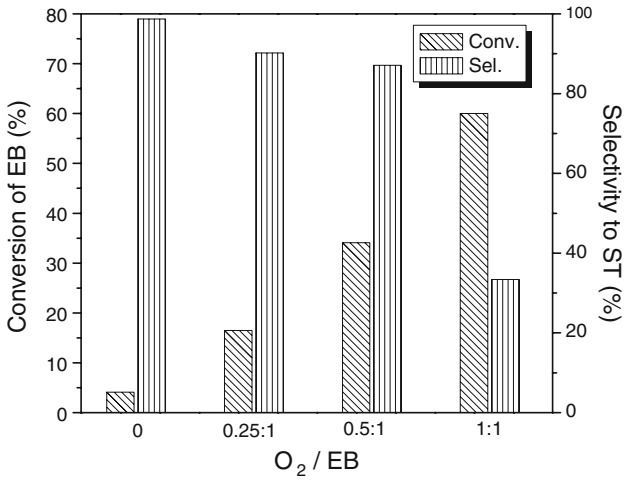

Fig. 5 Effect of O_2 concentration on the ODH performance of EB over CeO_2-450

remained high above 80%, with the CeO_2-450 sample being appreciably more selective than its counterparts obtained by calcination at higher temperatures. On the other hand, the CeO_2-700, CeO_2-800 and CeO_2-900 catalysts exhibited stable EB conversion in 5 h, i.e., ca. 22, 20, and 15%, respectively. As a contrast, the CeO_2-450 catalyst deactivated notably during the first 1 h, followed by a relatively stable EB conversion of ca. 27%. The initial decrease of the catalytic activity observed for the CeO_2-450 catalyst was likely caused by the loss of the surface area or growth of the CeO_2 particles. In fact, after reaction for 5 h, the BET surface area of the spent CeO_2-450 decreased to 152 $m^2\ g^{-1}$, corresponding to a crystallite size of ca. 7.3 nm as determined from the XRD result. At this juncture, it is interesting to note that no further deactivation was identified during an additional catalytic test of the

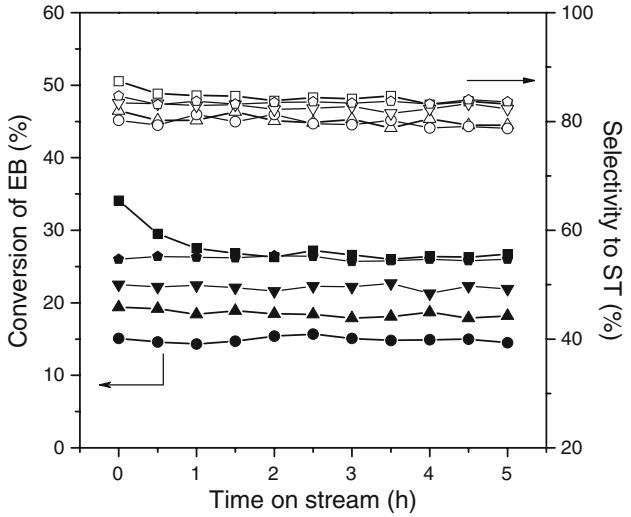

Fig. 6 EB conversion and selectivity of ST as a function time on stream obtained on ceria catalysts at 450 °C (square: CeO_2-450, down triangle: CeO_2-700, up triangle: CeO_2-800, circle: CeO_2-900, pentagon: spent CeO_2-450)

spent CeO_2-450 sample, which may be rationalized by the maintenance of the BET surface area (ca. 152 $m^2\ g^{-1}$) upon a first use of this material. Therefore, it can be concluded that the surface area or the particles size of CeO_2 plays an important role in its catalytic activity in the ODH of EB.

The catalytic performance of CeO_2-450 in the ODH of EB was also compared with those of other catalysts reported in the literature, as summarized in Table 3. It should be noted that the experimental conditions in the literature concerning the ODH of EB may deviate from each other. Nevertheless, a rough comparison is still feasible in the present study. As shown in Table 3, even under high space velocity and standard ($EB/O_2 = 2/1$) reaction conditions the CeO_2-450 sample exhibits a high catalytic performance. At 450 °C and total space velocity of 415 mL $g_{cat}^{-1}\ min^{-1}$, the obtained reaction rate for ST production is 6.1 mmol ST $g_{cat}^{-1}\ h^{-1}$ while the selectivity to ST is 84%. Apart from the 20%V–Mg–O catalyst, these values compare favorably with the results reported on most conventional metal oxide catalysts, over which the space velocities are much lower and the EB conversions are around 35% (see Table 3). Moreover, such ODH performance is comparable with those of the best carbon-based catalytic systems reported in the literature [5]. The above catalytic evaluation strongly suggested that the present as-synthesized mesostructured CeO_2-450 material with high surface area can serve as a promising catalyst for styrene synthesis from the ODH of EB.

With regard to the essential active phase of transition-metal-oxide and phosphate- based [1, 29] catalysts

Table 3 Comparison of the catalytic performances of different catalyst systems for ODH of EB

Catalyst	O/EB ratio	SV (mL g^{-1} min^{-1})	T (°C)	Conversion of EB (%)	Selectivity to ST (%)	Reaction rate (mmol-ST $g_{cat.}^{-1}$ h^{-1})	References
CeO_2-450[a]	0.5	415	450	27	84	6.1	This work
20%V–Mg–O	2	300	530	32	96	11.0	[9]
6%V/CeZr/SiO_2	3	30	400	20	92	2.0	[31]
$FePO_4$-A-450	2	61	440	24	86	0.16	[29]
$AlPO_4$	2	61	440	44	99	0.35	[29]
Popcarbon-900	1	200	400	48	86	6.2	[32]
CNF	1	50	400	56	85	1.27	[4]
CNF/graphite	5	83	400	29	80	1.04	[11]
OLC	1	250	510	92	68	8.38	[5]

[a] Reaction rate obtained after reaction for 5 h

previously reported for the ODH of ethylbenzene, it is widely accepted that the carbon deposits detected on these catalysts are indispensable for the genesis of "true" catalytically active sites for the ODH reaction. More specifically, it has been considered that the surface redox couples consisting of strongly basic adjacent (quinoidic) oxygen groups of the carbon deposits are responsible for the actual activity observed for these materials [1]. To elucidate the active phase in the present ceria-based catalytic system for the ODH of EB, TPO characterization of the used CeO_2-450 sample (at 5 h TOS) was conducted using flowing air in the TGA mode; the results are compared in Fig. 7. The fact that no carbon deposits could be detected over the used CeO_2-450 sample (see Fig. 7b) strongly indicates that the "carbon deposits" mechanism is not applicable for the present CeO_2-catalyzed ODH of EB.

On the other hand, it is well known that the selective oxidations of different hydrocarbons may proceed over ceria-based catalysts via a Mars-van Krevelen redox mechanism [30], in which the consumption and replenishment of the lattice surface oxygen species play a key role in the reaction process. To gain further insight into the nature of the ceria catalysts in relation to their ODH activity, the H_2 consumption of the low-temperature reduction peak in the TPR profiles are plotted against the EB conversion over the CeO_2 catalysts calcined at different temperatures as shown in Fig. 8. The variation in the H_2 consumption of the LT reduction peak shows a good correlation with the corresponding EB conversion. This indicates that the amount of surface lattice oxygen species on the ceria material contributes directly to the catalytic activity of CeO_2 in the ODH of EB reaction, permitting a rational explanation for the negative effect of calcination temperature on the performance of the catalyst. We therefore infer that the present ODH of EB over the CeO_2-based catalysts may proceed via a simple surface redox mechanism involving the Ce^{4+}/Ce^{3+}

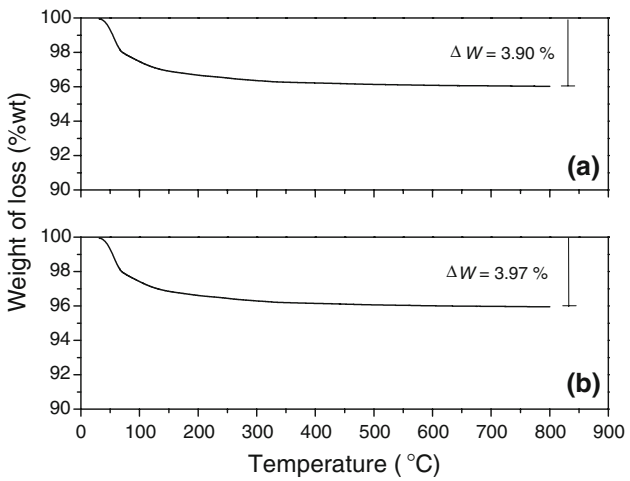

Fig. 7 TG curves of the fresh **a** and spent **b** CeO_2-450 samples

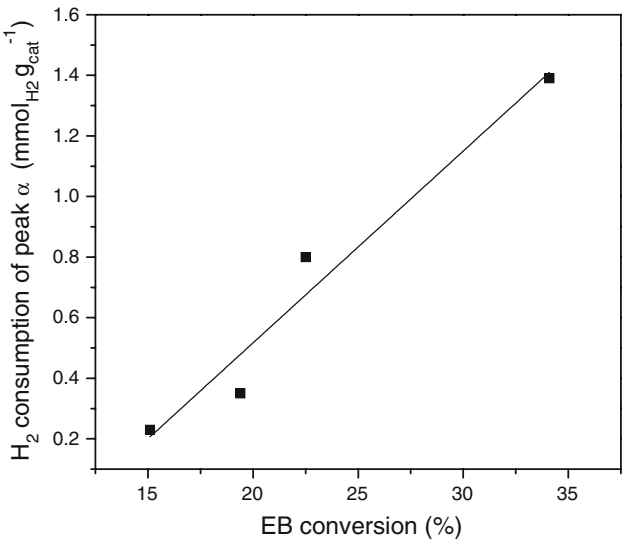

Fig. 8 Correlation between the catalytic activity with the H_2 consumption of peak α in TPR profiles of various ceria catalysts

couple, in which the catalyst undergoes reduction (by EB) and reoxidation (by O_2) cycles.

4 Conclusions

In summary, a new efficient mesostructured ceria catalyst featured with high surface area has been developed for the ODH of ethylbenzene using O_2 as the oxidant. The effect of calcination temperature on the catalytic performance of the ceria material was investigated. The best catalytic performance was obtained over the CeO_2-450 sample under a high space velocity condition, affording a steady STY of 6.1 mmol-ST g^{-1} h^{-1} at 450 °C. The superior performance of CeO_2-450 in the ODH of EB has been attributed to the high specific surface area and the well-developed mesostructure of this material. As a result, the ODH of EB could proceed much more effectively over the CeO_2-450 sample with enhanced low temperature redox capacities, thus leading to the significant enhancement of its performance for the ODH of EB.

Acknowledgments This work was financially supported by the National Natural Science Foundation of China (20633030, 20721063, 20803012, and 20873026), the National High Technology Research and Development Program of China (2006AA03Z336), and the National Basic Research Program of China (2009CB623506), Science & Technology Commission of Shanghai Municipality (08DZ2270500, 07QH14003) and the Committee of the Shanghai Education (06SG03).

References

1. Cavani F, Trifiro F (1995) Appl Catal A-Gen 133:219–239
2. Reddy BM, Rao KN, Reddy GK, Khan A, Park SE (2007) J Phys Chem C 111:18751–18758
3. Lee E (1973) Catal Rev 8:285–305
4. Zhao TJ, Sun WZ, Gu XY, Ronning M, Chen D, Dai YC, Yuan WK, Holmen A (2007) Appl Catal A-Gen 323:135–146
5. Su DS, Maksimova NI, Mestl G, Kuznetsov VL, Keller V, Schlögl R, Keller N (2007) Carbon 45:2145–2151
6. Kustrowski P, Segura Y, Chmielarz L, Surman J, Dziembaj R, Cool P, Vansant EF (2006) Catal Today 114:307–313
7. Tagiyev DB, Gasimov GO, Rustamov MI (2005) Catal Today 102–103:197–202
8. Craciun R, Dulamita N (1999) Ind Eng Chem Res 38:1357–1363
9. Oganowski W, Hanuza J, Kepiski L (1998) Appl Catal A-Gen 171:145–154
10. Keller N, Maksimova NI, Roddatis VV, Schur M, Mestl G, Butenko YV, Kuznetsov VL, Schlögl R (2002) Angew Chem Int Ed Engl 41:1885–1888
11. Delgado JJ, Su DS, Rebmann G, Keller N, Gajovic A, Schlögl R (2006) J Catal 244:126–129
12. Li P, Li T, Zhou JH, Sui ZJ, Dai YC, Yuan WK, Chen D (2006) Micropor Mesopor Mat 95:1–7
13. Rinaldi A, Zhang J, Mizera J, Girgsdies F, Wang N, Hamid SBA, Schlögl R, Su DS (2008) Chem Commun 48:6528–6530
14. Bernal S, Blanco G, Cauqui MA, Corchado MP, Larese C, Pintado JM, Rodriguez-Izquierdo JM (1999) Catal Today 53:607–612
15. Trovarelli A, de Leitenburg C, Boaro M, Dolcetti G (1999) Catal Today 50:353–367
16. Trovarelli A, Dolcetti G, Deleitenburg C, Kaspar J, Finetti P, Santoni A (1992) Journal of the Chemical Society-Faraday Transactions 88:1311–1319
17. Monteiro RS, Dieguez LC, Schmal M (2001) Catal Today 65:77–89
18. Andreeva D, Ivanov I, Ilieva L, Abrashev MV (2006) Appl Catal A-Gen 302:127–132
19. Ye XN, Yue YH, Miao CX, Xie ZK, Hua WM, Gao Z (2005) Green Chem 7:524–528
20. Luo MF, Ma JM, Lu JQ, Song YP, Wang YJ (2007) J Catal 246:52–59
21. Liu Q, Wang LC, Chen M, Cao Y, He HY, Fan KN (2009) J Catal 263:104–113
22. Wang YJ, Ma JM, Luo MF, Fang P, He M (2007) J Rare Earths 25:58–62
23. Terribile D, Trovarelli A, Llorca J, de Leitenburg C, Dolcetti G (1998) J Catal 178:299–308
24. Scire S, Minico S, Crisafulli C, Satriano C, Pistone A (2003) Appl Catal B-Environ 40:43–49
25. Venezia AM, Pantaleo G, Longo A, Di Carlo G, Casaletto MP, Liotta FL, Deganello G (2005) J Phys Chem B 109:2821–2827
26. Blank JH, Beckers J, Collignon PF, Rothenberg G (2007) Chemphyschem 8:2490–2497
27. Giordano F, Trovarelli A, de Leitenburg C, Giona M (2000) J Catal 193:273–282
28. Bruce LA, Hoang M, Hughes AE, Turney TW (1996) Appl Catal A-Gen 134:351–362
29. Bautista FM, Campelo JM, Luna D, Marinas JM, Quiros RA, Romero AA (2007) Appl Catal B-Environ 70:611–620
30. Grasselli RK (2002) Top Catal 21:79–88
31. Reddy BM, Lakshmanan P, Loridant P, Yamada Y, Kobayashi T, Lopez-Cartes C, Rojas TC, Fernandez A (2006) J Phys Chem B 110:9140–9147
32. Wang LF, Zhang J, Su DS, Ji YY, Cao XJ, Xiao FS (2007) Chem Mater 19:2894–2897